PLOS ONE

RESEARCH ARTICLE

Intramolecular *ex vivo* Fluorescence Resonance Energy Transfer (FRET) of Dihydropyridine Receptor (DHPR) β_{1a} Subunit Reveals Conformational Change Induced by RYR1 in Mouse Skeletal Myotubes

Dipankar Bhattacharya[1¤], Andrew Mehle[2], Timothy J. Kamp[1], Ravi C. Balijepalli[1]*

1 Cellular and Molecular Arrhythmia Research Program, Department of Medicine, University of Wisconsin-Madison, Wisconsin, United States of America, **2** Department of Medical Microbiology and Immunology, University of Wisconsin-Madison, Wisconsin, United States of America

¤ Current Address: Department of Medicine, Division of Liver Diseases, Mount Sinai School of Medicine, New York, New York, United States of America
* rcb@medicine.wisc.edu

OPEN ACCESS

Citation: Bhattacharya D, Mehle A, Kamp TJ, Balijepalli RC (2015) Intramolecular *ex vivo* Fluorescence Resonance Energy Transfer (FRET) of Dihydropyridine Receptor (DHPR) β_{1a} Subunit Reveals Conformational Change Induced by RYR1 in Mouse Skeletal Myotubes. PLoS ONE 10(6): e0131399. doi:10.1371/journal.pone.0131399

Editor: Nicole Beard, University of Canberra, AUSTRALIA

Received: September 2, 2014

Accepted: June 2, 2015

Published: June 26, 2015

Data Availability Statement: All relevant data are within the paper.

Funding: This work was supported by a grant from the National Institutes of Health R01 grants HL105713 to RCB, HL078878 and AR046448 to TJK. The funders had no role in study design, data collection and analysis, decision to publish, or preparation of the manuscript.

Competing Interests: The authors have declared that no competing interests exist.

Abstract

The dihydropyridine receptor (DHPR) β_{1a} subunit is essential for skeletal muscle excitation-contraction coupling, but the structural organization of β_{1a} as part of the macromolecular DHPR-ryanodine receptor type I (RyR1) complex is still debatable. We used fluorescence resonance energy transfer (FRET) to probe proximity relationships within the β_{1a} subunit in cultured skeletal myotubes lacking or expressing RyR1. The fluorescein biarsenical reagent FlAsH was used as the FRET acceptor, which exhibits fluorescence upon binding to specific tetracysteine motifs, and enhanced cyan fluorescent protein (CFP) was used as the FRET donor. Ten β_{1a} reporter constructs were generated by inserting the CCPGCC FlAsH binding motif into five positions probing the five domains of β_{1a} with either carboxyl or amino terminal fused CFP. FRET efficiency was largest when CCPGCC was positioned next to CFP, and significant intramolecular FRET was observed for all constructs suggesting that *in situ* the β_{1a} subunit has a relatively compact conformation in which the carboxyl and amino termini are not extended. Comparison of the FRET efficiency in wild type to that in dyspedic (lacking RyR1) myotubes revealed that in only one construct (H458 CCPGCC β_{1a} -CFP) FRET efficiency was specifically altered by the presence of RyR1. The present study reveals that the C-terminal of the β_{1a} subunit changes conformation in the presence of RyR1 consistent with an interaction between the C-terminal of β_{1a} and RyR1 in resting myotubes.

Introduction

Contraction of a skeletal muscle cell is initiated by a depolarization, which in turn triggers an increase in cytosolic Ca^{2+}. The process that transduces membrane depolarization into a cytosolic Ca^{2+} increase is controlled by two highly specialized ion channel complexes, namely the dihydropyridine receptor (DHPR) L-type Ca^{2+} channel in the sarcolemma and the ryanodine receptor type 1 (RyR1) present in the sarcoplasmic reticulum. In skeletal muscle, protein-protein interactions between the pore subunit of the DHPR (α_{1S}) and RyR1 are extensive, [1–9]. The α_{1S} subunit has the familiar topology of a four-repeat voltage-gated channel in which long loops, of ~50 to 150 residues, connect the internal repeats [10]. 3-D reconstructions of skeletal DHPR particles and models of DHPR tetrads suggest that the cytosolic loops of the pore subunit are in intimate contact with the foot structure of RyR1 [11, 12]. The protein-protein interactions between the cytosolic $ß_{1a}$ subunit of the DHPR and RyR1 have also been established [13, 14]; however, the precise role of DHPR $ß_{1a}$ in excitation-contraction coupling is not well defined.

Multiple functional roles of DHPR ß subunits have been identified. DHPR ß subunits strongly modulate the gating of Ca^{2+} channels and also promote the trafficking of channels to the surface membrane [15–22]. Four different genes encode DHPR ß subunits in mammals with multiple splice variants identified for each gene. Knockout of the mouse $ß_1$ gene using gene targeting results in the complete absence of excitation-contraction (E-C) coupling in skeletal muscle, which can be rescued by heterologous expression of $ß_1$ in knockout myotubes [23]. The impact of $ß_1$ knockout in the mouse model appears to be primarily due to a lack of membrane trafficking of α_{1S} to the sarcolemma [24]. Expression studies in $ß_1$ KO myotubes have demonstrated that a wide range of different ß subunit isoforms promote membrane trafficking of α_{1S} rescuing L-type Ca^{2+} currents, but only $ß_{1a}$ and $ß_{1c}$ can specifically rescue skeletal muscle type excitation-contraction coupling [25–28]. Thus the $ß_1$ subunit plays a highly specific role in skeletal muscle E-C coupling in addition to its role in promoting membrane trafficking and modulating gating of the DHPR channel complex.

The voltage-dependent Ca^{2+} channel auxiliary ß subunits are composed of 5 domains including a variable N-terminus, a conserved SH3 domain, a variable linker domain, a conserved GK domain and a variable C-terminus. The core structures of several ß subunits have been solved using X-Ray crystallography and exhibit features representative of the membrane-associated guanylate kinase (MAGUK) superfamily of proteins [29–31]. However, the structures of the N- and C-termini of ß subunits are unknown and how these regions relate to the core of the ß subunit has not been determined. Furthermore, information regarding the conformations and relationship of the ß subunits domains in living cells is not available.

Measurement of fluorescence resonance energy transfer (FRET) efficiency between a donor and an acceptor can provide information on proximity relationships between structural domains of proteins [32]. In this study, we have used an *ex vivo* FRET assay to determine proximity relationships between domains of the $ß_{1a}$ subunit as a means to examine the domain organization of $ß_{1a}$ in living skeletal muscle cells. We have chosen the biarsenical fluorescein derivative FlAsH which exhibits fluorescence upon binding to specific tetracysteine motifs [33–35] as a FRET acceptor and enhanced cyan fluorescent protein (CFP) as a FRET donor [33–37]. Our previous studies and those of others have demonstrated efficient CFP/FlASH tetracysteine FRET in living cells [35] [36] [37]. Tagging ß subunits with fluorescent proteins such as CFP, at least at the N- or C-terminus, does not affect function [38]. On the other hand the advantage of using FlAsH is that the tetracysteine domain required for FlAsH binding is very small and less intrusive than other acceptors of choice such as YFP, and so the inserted tetracysteine motif is much less likely to perturb intrinsic biological function of the protein [35,

36]. Furthermore, i) FlAsH binds to proteins tagged with the CCPGCC motif with picomolar affinity; ii) the reagent is cell-permeant; iii) bound FlAsH can be effectively displaced with 1,2-ethanedithiol (EDT); and iv) unbound FlAsH is, for all practical purposes, non-fluorescent [34]. Thus, a FlAsH labeling protocol in cultured cells is easy to implement, and FRET efficiency can be directly quantified from the quenching of CFP emission in the presence and absence of FlAsH [39]. However, FlAsH suffers from two potential limitations: accessibility of FlAsH to the tetracysteine site and background labeling of myotubes [40] that, in principle, could compromise the measurement of the FRET efficiency. In the present work, we have directly addressed both issues. We detected robust intramolecular FRET at 10 donor/acceptor positions within the DHPR $ß_{1a}$ subunit and identified a single donor/acceptor position in which FRET efficiency specifically changed in response to RyR1 expression.

Materials and Methods

Ethical approval

The procedure for mouse skeletal myotube isolation was fully approved by the Institutional Animal Care and Use Committee of the University of Wisconsin School of Medicine and Public Health.

Mouse models. Heterozygous mice $RyR1^{+/-}$ were a gift of Dr. Hiroshi Takeshima of International Institute for Advanced Studies, Japan [41]. Outbred C57BL/6 mice (Charles River, MA) were used to generate colonies of heterozygous dyspedic ($RyR1^{+/-}$) mice. RyR1 null ($RyR1^{-/-}$) mice were generated by interbreeding of heterozygous parents. PCR primers 5' GGA CTG GCA AGA GGA CCG GAG 3' and 5' GGA AGC CAG GGC TGC AGG TGA GC 3' were used to amplify a 400-bp fragment of the WT RyR1 allele. PCR primers 5' GGA CTG GCA AGA GGA CCG GAG 3' and 5' CCT GAA CGA GAT CAG CCT CTG TTC C 3' were used to amplify a 300-bp fragment of the KO RyR1 allele. The PCR cycles for both RyR1 alleles are as follows: initial denature at 94°C for 5 min followed by 35 cycles of 1 min at 94°C, 1 min at 57°C and 1 min at 72°C and finally one cycle for 10 min at 72°C.

Heterozygous DHPR $ß_1^{+/-}$ mice were generated at the transgenic mouse core facility at the University of Wisconsin-Madison [23]. $ß_1$ null ($ß_1^{-/-}$) null mice were obtained by interbreeding of heterozygous parents. PCR primers 5' GAG AGA CAT GAC AGA CTC AGC TCG GAG A 3' and 5' ACA CCC CCT GCC AGT GGT AAG AGC 3' were used to identify a 250 bp fragment of WT ß1 allele. PCR primers 5`ACA CCC CCT GCC AGT GGT AAG AGC 3`and 5`ACA ATA GCA GGC ATG CTG GGG ATG 3' to amplify a 197 bp fragment for identifying the KO $ß_1$ allele. The PCR cycles for both DHPR $ß_1$ alleles are as follows: initial denature at 94°C for 2 min followed by 30 cycles of 30 sec at 94°C, 45 sec at 60°C and 1 min at 72°C and finally one cycle for 10 min at 72°C.

CFP/tetracysteine cDNAs. For calibration of *ex vivo* FRET measurements, we used a CFP-tetracysteine concatemer. The 17 amino acid long FlAsH binding motif AEAAAR-EACCPGCCARA (here on referred as CCPGCC) as previously described [42] was introduced in frame in the C-terminus of ECFP by PCR techniques. The PCR product was directly cloned into ECFP-C1 vector (Clontech, CA)(construct 1). For determination of relative proximity within the DHPR $ß_{1a}$ subunit, we inserted the FlAsH binding motif at five positions in the $ß_{1a}$ sequence and fused CFP to either the N-terminus or C-terminus of $ß_{1a}$ (constructs 8, 12 and 14 to 21). Full-length $ß_{1a}$ (1–524) (GenBank accession No. NM_031173) was cloned in frame to both ECFP-N1 and ECFP-C1 vectors (Clontech, CA) for fusion of CFP to the N- or C-termini of $ß_{1a}$. Insertion of the above described 17-amino acid FlAsH binding motif in different positions was done by two-step PCR strategies. Six to nine base primers were designed to match cloning sites, and to introduce the FlAsH-binding motif. PCR products were cloned into

ECFP-N1- ß$_{1a}$ (constructs 8, and 14 to 17) and ECFP-C1- ß$_{1a}$ (constructs 12 and 18 to 21) vectors at the following sites: *EcoRI/MluI* sites for inserting the 17-mer immediately before ß$_{1a}$ M1, after ß$_{1a}$ Q57, and after ß$_{1a}$ P249; *MluI/SalI* sites for inserting the 17-mer after ß$_{1a}$ H458 and after ß$_{1a}$ M524. The resulting products were confirmed by sequencing. To confirm the specificity of FlAsH labeling in the myotubes system, we generated and tested five different CFP-teracystine concatemer constructs (constructs 1–4,) and a CFP construct without any tetracysteine motif (construct 5). To determine the FlAsH accessibility we generated and tested five additional constructs with the insertion of CFP-CCPGCC motif in five different domains (as mentioned above) of full-length ß$_{1a}$ (constructs 8 to 12). We also made two individual constructs either CFP fused (construct 6) or CCPGCC fused (construct 7) in the N-terminal of β$_{1a}$.

Primary myotube cultures. Primary cultures of myotubes were prepared from enzyme-digested mouse hind limbs of wild type, RyR1 KO (dyspedic) and ß$_1$ KO embryos (E18) as described earlier [43],[44]. Briefly, the muscles were dissected from fetuses and treated with 0.25% (w/v) trypsin, 0.05% (w/v) pancreatin and 0.1% (v/v) penicillin-streptomycin followed by centrifugation and collection of the cells. Mononucleated cells were resuspended in DMEM containing low glucose, 10% horse serum, 10% FBS, 2% chicken serum extract and 0.1% (v/v) penicillin-streptomycin. After plating the cells (~1X10^4 cells/dish) on 1% gelatin coated 35 mm plastic dishes, the cultures were grown at 37°C in 8% CO_2 incubator for five to six days. At the myoblast fusion stage, the medium was replaced with DMEM, 10% horse serum, 1.25% chicken embryo extract and 0.1% penicillin-streptomycin, and CO_2 was decreased to 5%. All the transfections were performed at the myoblast fusion stage with TransIT-LT1 (Mirus Corporation, WI). Cells were incubated with transfection solution containing LT1 and cDNA of interest (5:1 μg ratio) for 3 hours. In case of RyR1 transfected dyspedic myotubes, a separate expression vector encoding the T cell membrane antigen CD8 were mixed, as a transfection marker, and triply transfected [H485 CCPGCC ß$_{1a}$ CFP (construct 21), RyR1 and CD8 constructs] with the LT1. *Ex vivo* FRET and whole-cell analyses of Ca^{2+} currents were performed after 72 hours following transfection. Triply transfected cells were recognized by incubation with CD8 antibody-coated beads (Dynal, Norway) and the transfection efficiency was ~80%.

Electrophysiology. Whole-cell voltage-clamp electrophysiology was performed on myotubes using Axopatch 200B amplifier (Axon Instruments, Foster City, CA) with pClamp 7, software. The patch pipettes were pulled from thin walled borosilicate glass capillaries (World Precision Instruments, Inc., Sarasota FL) on Sutter P-87 micropipette puller (Sutter Instrument Co) and polished using microforge MF900 (Narishige). All the experiments were carried out at room temperature with pipette resistance of 1.5–2.5MΩ [44]. The external solution was (in mM) 130 tetraethylammonium-methanesulfonate, 10 $CaCl_2$, 1 $MgCl_2$, 10 Hepes-tetraethylammonium (OH), pH 7.4. The pipette solution was (in mM) 140 Cs-aspartate, 5 $MgCl_2$, 5 EGTA, 10 4-morpholinepropanesulfonic acid-CsOH (pH 7.2).

FlAsH labeling and myotube fluorescence. FlAsH labeling was performed with modifications to the protocols described previously [34, 36]. The culture plates were thoroughly rinsed with a rodent Ringer's solution (in mM: 146 NaCl, 5 KCl, 2 $CaCl_2$, 1 $MgCl_2$, 10 HEPES, pH 7.4) supplemented with 10 mM glucose and 1 mM Na-pyruvate. The cells were equilibrated for 30 minutes in the dark by adding 2 ml of rodent Ringer's solution in plates. Each plate was covered with 250 μl of a freshly-made loading solution consisting of 10 μM EDT (Aldrich, WI) and 1 μM FlAsH-EDT_2 (named Lumio Green from Invitrogen, CA) in rodent Ringer's solution and incubated at room temperature for 2 hours in the dark with gentle shaking. FlAsH loaded myotubes were thoroughly washed with rodent Ringer's solution before imaging. Myotube epifluorescence was captured with a cooled CCD DP-70 camera (Olympus) using a 20X/0.95 NA water-immersion objective in an upright Olympus BX51 water-immersion microscope. The sample was excited using 100W Hg lamp and light filtered with standard band-pass excitation/

emission filter cubes (ex436/20 nm, em480/30 nm, dichroic455 for CFP, and ex500/20 nm, em535/30 nm, dichroic515 for fluorescein). Image acquisitions of emission of both CFP and FlAsH before and after clearance of FlAsH with EDT were made as described earlier [36]. In brief, one cell per dish was selected and the position of the dish was fixed on microscope stage once the region of interest was selected and imaged. FlAsH removal was accomplished by superfusion with EDT (7.5 mM final concentration) and 2% DMSO in same rodent Ringer's solution. Cells were washed carefully under direct microscopic visualization, and only cells that showed no detectable change in localization were analyzed. This allowed imaging from same area of the cells before and after FlAsH clearance. Within ten minutes after adding EDT, fluorescein intensity in the myotubes was below detectable levels, and the cell was imaged again. Image analysis was performed using the ImageJ software (Rasband, W.S., ImageJ, U. S. National Institutes of Health, Bethesda, Maryland, USA, http://imagej.nih.gov/ij/, 1997–2014) and [45]. The FRET measurements and analysis were accomplished according to a previously described method by us [36]. A scale of 0 to 225 was used for analyzing of mean pixel intensities of the cells by selecting low to mid expressions. The FRET ratio was calculated by CFP emission after FlAsH loading and after EDT)/(CFP emission after FlAsH loading and before EDT followed by calculation of FRET efficiency = 1-[1/(FRET ratio)] [39]. The FRET efficiency is directly related to the distance between CFP and FlAsH fluorophores according to Förster theory [46].

Structural model. The $ß_{1a}$ subunit structure was predicted with Phyre2 [47]. The highest confidence model was obtained using $ß_3$ as a template (PDB 1VYU) [29, 47]. The model includes residues 72–175 in the SH3 domain and residues 265-322/383-458 in the GK domain.

Statistics. Data are presented as means ± standard error of the mean. Comparisons between two groups were done using student's t-test. For multiple comparisons, ANOVA was performed with subsequent Bonferroni t-test comparing test groups to the control group. Statistical significance was defined at a value of $p<0.05$.

Results

FlAsH-mediated ex vivo FRET in myotubes

For validation of the FlAsH-based ex vivo FRET in skeletal myotubes, we made several fusion constructs of CFP and the tetracysteine motifs designed to bind FlAsH [36, 42]. The CFP-CCXXCC concatemers were expressed in normal myotubes for 72 hours followed by 2 hours of labeling with 1 μM FlAsH-EDT_2 in rodent Ringer's solution. Following FlAsH labeling, cells were incubated with 7.5 mM EDT to track the increase in CFP emission (decrease in FRET) due to the removal of bound FlAsH. Fig 1A shows the changes in donor and acceptor fluorescence in myotubes expressing the CFP-CCPGCC concatemer (construct 1) during the FlAsH labeling protocol. CFP emission decreases after incubation with FlAsH (Fig 1A middle panel), and recovers following FlAsH removal with 7.5 mM EDT (Fig 1A right panel). FlAsH emission is drastically reduced after EDT treatment. The line-scans in Fig 1B show pixel intensity across the width of a cell in the conditions described above in the donor and acceptor channels. To ensure reproducibility and to conform to the definition of FRET efficiency [39], we only focused on cells in which FlAsH removal was substantial (less than 10% residual FlAsH emission after EDT incubation). In the cells with substantial FlAsH unloading by EDT, the CFP emission increased ~2 fold (Fig 1C). The increase in donor emission with concomitant decrease in acceptor emission is a telltale sign of FRET [39]. A robust FRET process, with an efficiency of 0.52 ± 0.04 was measured in the CFP-CCPGCC (construct 1) concatemer expressed in myotubes.

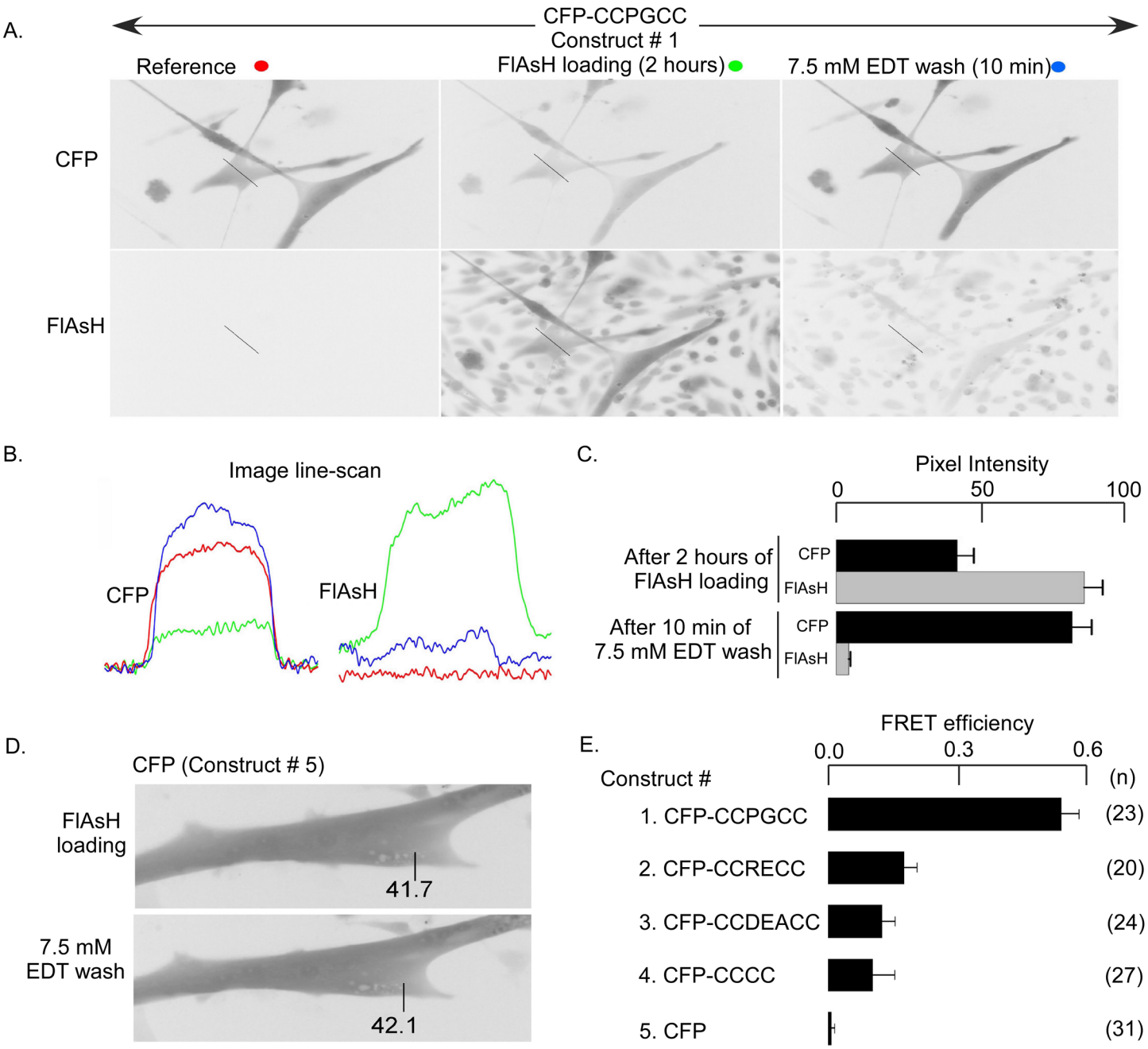

Fig 1. FRET signals in myotubes expressing CFP-CCXXCC and WT CFP. (A) CFP-CCPGCC concatamer (construct 1) transfected myotubes show a high level of CFP expression as indicated by fluorescence in the CFP channel. Before FlAsH loading there was no fluorescence in the FLUO channel for the reference condition (red circle, left panels). After 2 hrs of incubation in 1 μM FlAsH to load the tetracysteine motif, fluorescence in the CFP channel decreased and in the FLUO channel increased (green circle, middle panel). Incubation with 7.5 mM EDT for 10 minutes to displace FlAsH from the tetracysteine tag reversed the fluorescence changes back toward the reference conditions (blue circle, right panels). (B) Pixel intensity of a line scan across the myotube (straight line indicated in each panel of A) in the CFP versus FLUO channels. Colors of traces correspond to color markings in A. (C) Summary of mean pixel intensities of CFP-CCPGCC concatamer (construct 1) expressed in myotubes. (D) WT-CFP (construct 5) transfected myotubes (without the tetracysteine tag) show no change in CFP fluorescence after 1 μM FlAsH loading or after 7.5 mM EDT wash. The number represents the fluorescence intensity (CFP) of a particular region in the myotube. (E) FRET vs FlAsH binding sequences showing CFP-CCPGCC (construct 1) FlAsH complex. Highest FRET efficiency (0.52 ± 0.04) was observed with CFP-CCPGCC (construct 1) than CFP-CCRECC (construct 2, 0.17±0.03), CFP-CCDAECC (construct 3, 0.12 ± 0.03), CFP-CCCC (construct 4, 0.10 ± 0.05) or untagged CFP-CFP (construct 5, 0.07 ± 0.01). Total number of cells (n) analyzed is shown within brackets.

doi:10.1371/journal.pone.0131399.g001

To confirm that the ex vivo FRET signal involved the engineered tetracysteine and not spurious FlAsH acceptors at non-specific sites, we tested CCXXCC tags with different affinities for FlAsH [36, 42], as well as CFP without the tetracysteine tag (Fig 1E construct 1 to 5). The measured FRET efficiency correlated well with the reported affinities of FlAsH for tetracysteine binding sites, which are 4 pM for CCPGCC, 70 pM for CCRECC, 1,800 pM for CCCC and 92,000 pM for CCDEACC [42]. Furthermore, FRET was undetectable in an untagged CFP (Fig 1D and 1E, construct 5). The latter result is important since it confirmed that CFP bleaching during image acquisition and incubation with EDT were insignificant. Thus, the FRET signal only involves the donor and FlAsH acceptor bound to the tetracysteine motif.

Intramolecular FRET of DHPR $ß_{1a}$ subunit in myotubes

After validating the FlAsH-based *ex vivo* FRET system using the CFP-CCPGCC concatemers in myotubes, we sought to evaluate FRET in tagged $ß_{1a}$ subunits. Control experiments revealed that FRET was not detected in the CFP- $ß_{1a}$ fusion that lacked the tetracysteine tag (construct 6) (Fig 2G and 2H), demonstrating that nonspecific binding of FlAsH does not yield any spurious FRET. We also tested for intermolecular FRET between $ß_{1a}$ subunits, given that ß subunits can exhibit intermolecular interaction under certain conditions [48–50]. Co-expressing N-terminal CFP- $ß_{1a}$ and CCPGCC- $ß_{1a}$ in wild type myotubes (Fig 2A) did not result in detectable FlAsH-mediated FRET (Fig 2G and 2H; co-transfected with constructs 6 and 7). Therefore, expression of constructs containing both FRET donor and acceptor in the same $ß_{1a}$ molecule will report intramolecular proximity relationships without the complication of intermolecular FRET between different $ß_{1a}$ subunits.

To determine if accessibility of FlAsH to the CCPGCC motif is a limitation in expressed $ß_{1a}$ subunits, we inserted the CFP-CCPGCC concatemer in five different positions (Fig 2 constructs 8 to 12): the M1 (N-terminal), Q57 (junction of N-terminus and SH3 domains), P249 (the linker between the SH3 and GK domains), or H458 (junction between GK domain and C-terminus;) and M524 (C-terminal). These constructs were expressed independently in wild type myotubes (Fig 2B–2F). FRET efficiency at these five positions in wild type myotubes was similar (Fig 2H constructs 8 to 12) to that of the free concatemer (Fig 1E, construct 1). Thus, the tertiary structure of $ß_{1a}$ does not hinder access of FlAsH to the tetracysteine site. Furthermore, all of these five $ß_{1a}$ CFP-CCPGCC constructs result in large inward $I_{Ca,L}$ when expressed in ß KO myotubes (Fig 3 constructs 8 to 12) which demonstrates the presence of functional ß subunits.

To map the domains of $ß_{1a}$ by FRET we kept the donor (CFP) position fixed at either the N-terminus or C-terminus and introduced the acceptor (CCPGCC motif) at the same five critical positions described above in $ß_{1a}$ molecule (constructs 8, 12 and 14 to 21). FRET efficiency measurements were conducted in wild type as well as dyspedic (lacking RyR1) myotubes. In general, comparatively weaker FRET was detected when CFP and the tetracysteine tag were separated by intervening $ß_{1a}$ sequence compared to inserted CFP-CCPGCC concatemers; however, for each of the inserted positions high FRET efficiency was observed (Fig 4A and 4B). The results were indistinguishable between wild type and dyspedic myotubes for all constructs except for a significant difference ($p<0.001$) in case of H458 CCPGCC $ß_{1a}$-CFP (construct 21). The FRET efficiency at this location was 0.12 ± 0.01 in wild type myotubes and 0.19 ± 0.01 in dyspedic myotubes (Fig 4B, construct 21 and Table 1). These data indicate a conformational change in the C-terminus of $ß_{1a}$ induced by the presence of RyR1. They lower FRET between excitation pairs at H458 CCPGCC and the C-terminus CFP further suggests that the C-terminal region assumes a more extended conformation in the presence of RyR1.

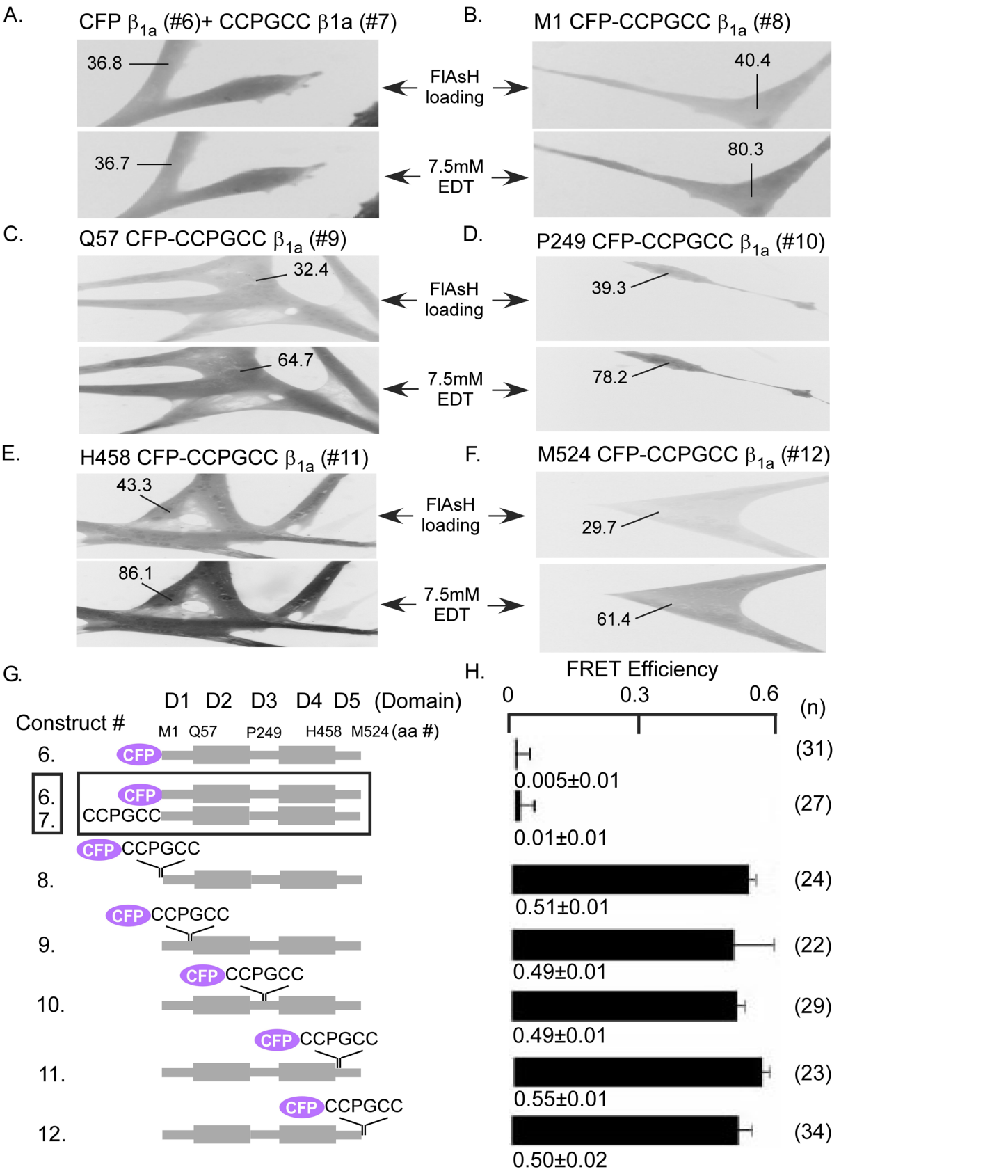
A.
CFP β1a (#6)+ CCPGCC β1a (#7)
36.8
36.7
FlAsH loading
7.5mM EDT
B.
M1 CFP-CCPGCC β1a (#8)
40.4
80.3
C.
Q57 CFP-CCPGCC β1a (#9)
32.4
64.7
FlAsH loading
7.5mM EDT
D.
P249 CFP-CCPGCC β1a (#10)
39.3
78.2
E.
H458 CFP-CCPGCC β1a (#11)
43.3
86.1
FlAsH loading
7.5mM EDT
F.
M524 CFP-CCPGCC β1a (#12)
29.7
61.4
G.
D1 D2 D3 D4 D5 (Domain)
Construct #
M1 Q57 P249 H458 M524 (aa #)
6.
CFP
6.
7.
CFP
CCPGCC
CFP CCPGCC
8.
CFP CCPGCC
9.
CFP CCPGCC
10.
CFP CCPGCC
11.
CFP CCPGCC
12.
H.
FRET Efficiency
0
0.3
0.6
(n)
(31)
0.005±0.01
(27)
0.01±0.01
(24)
0.51±0.01
(22)
0.49±0.01
(29)
0.49±0.01
(23)
0.55±0.01
(34)
0.50±0.02

Fig 2. FRET signals from $ß_{1a}$ subunits incorporating the CFP-CCPGCC concatamer in different domains or doubly transfected CFP and CCPGCC tags expressed in WT myotubes. (A) Myotubes co-transfected with CFP- $ß_{1a}$ (construct 6) and CCPGCC- $ß_{1a}$ (construct 7), constructs demonstrate unchanged FRET efficiency after FlAsH clearance with 7.5 mM EDT indicating that $ß_{1a}$ intermolecular interactions do not contribute to FRET in the present study. Myotubes individually transfected with the CFP-CCPGCC concatemers (B) M1 CFP-CCPGCC $ß_{1a}$ (construct 8), (C) Q57 CFP-CCPGCC $ß_{1a}$ (construct 9), (D) P249 CFP-CCPGCC $ß_{1a}$ (construct 10), (E) H458 CFP-CCPGCC $ß_{1a}$ (construct 11) or (F) M524 CFP-CCPGCC $ß_{1a}$ (construct 12) show ~2 fold FRET efficiency after FlAsH clearance with 7.5mM EDT. The numbers indicated represents the fluorescence intensity of the region in the myotubes before and after FlAsH clearance with EDT for FRET measurements. (G) Schematic diagrams of tagged $ß_{1a}$ constructs (constructs 6 to 12) that were used to assess the accessibility of FlAsH to tertracycteine tags incorporated in different domain of $ß_{1a}$. (H) Comparison of the FRET efficiencies for different $ß_{1a}$ constructs (constructs 6 to 12) expressed in WT myotubes that shows in panel A to G with number of tested cells for each group in parentheses. Mean FRET efficiencies ± standard errors are shown.

doi:10.1371/journal.pone.0131399.g002

The H458 CCPGCC $ß_{1a}$-CFP construct (construct 21) was then subjected to additional analysis given the difference in FRET observed between wild type and dyspedic myotubes.

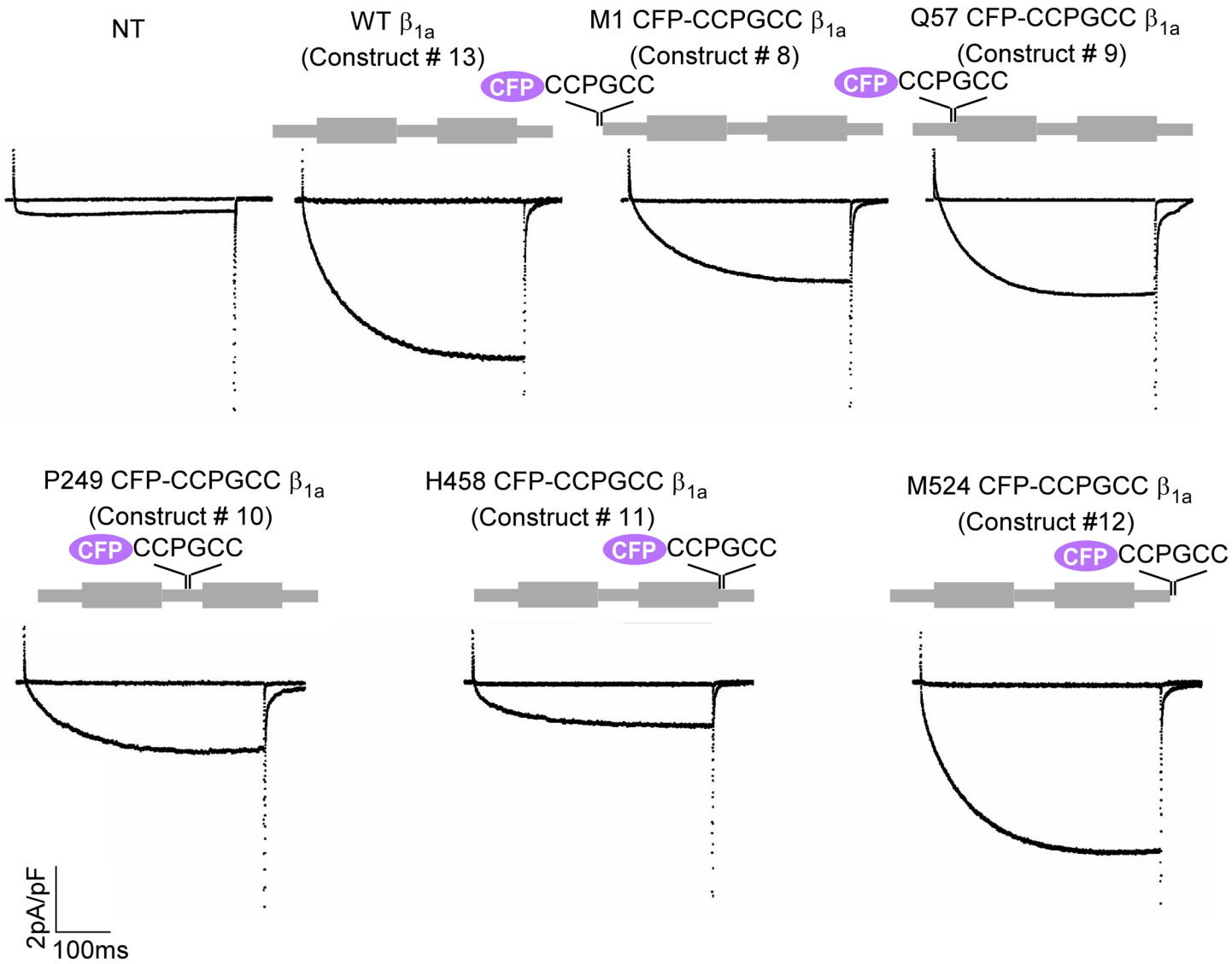

Fig 3. Representative Ca^{2+} current traces resulting from 200 ms test depolarizations to –30 mV and +30 mV in $ß_1$ KO myotubes expressing wild-type $ß_{1a}$ (WT $ß_{1a}$ construct 13) and the $ß_{1a}$ CFP-CCPGCC concatemer constructs (constructs 8 to 13) used in Fig 2B–2F or non-transfected (NT) controls.

doi:10.1371/journal.pone.0131399.g003

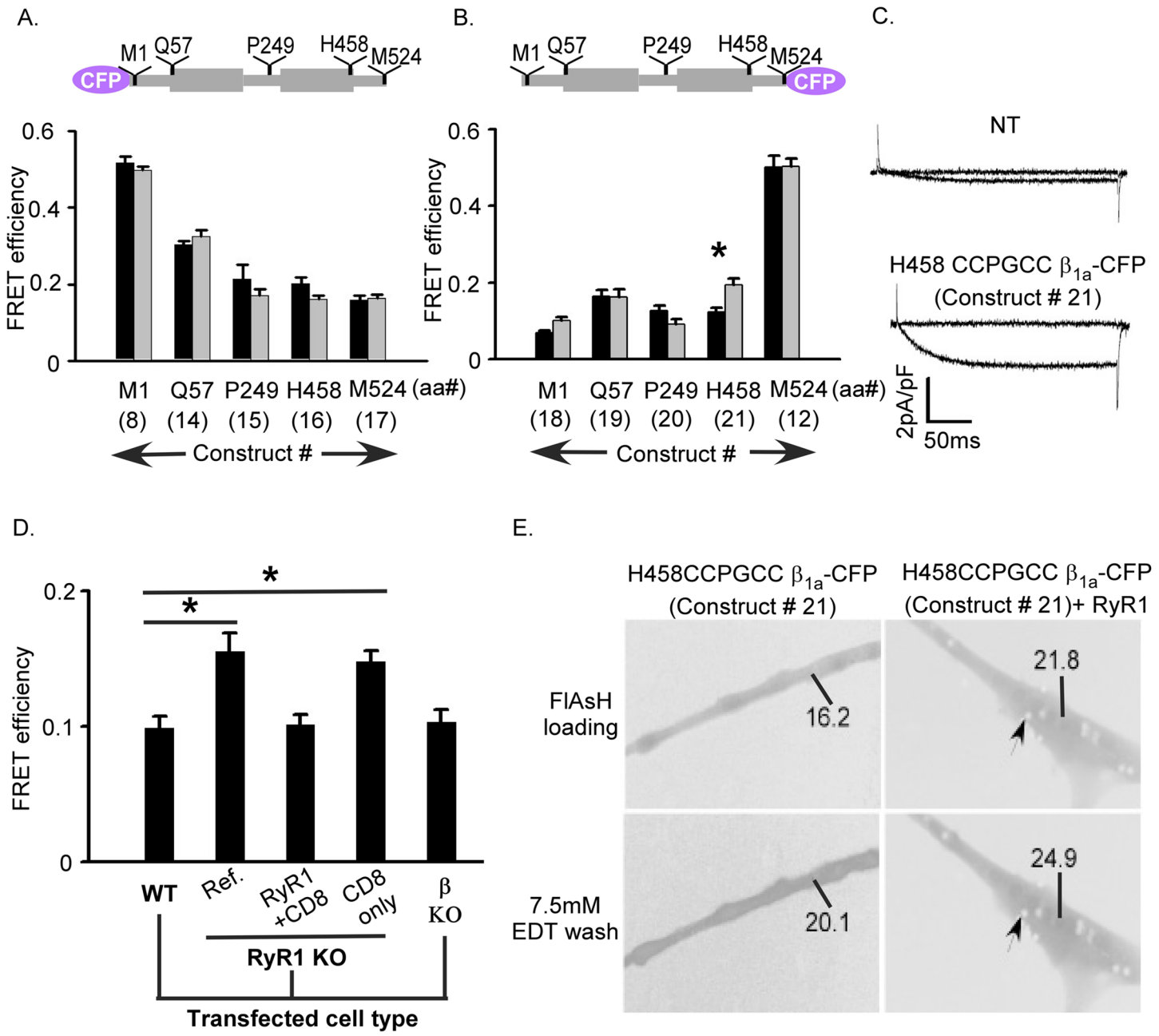

Fig 4. Intramolecular FRET in the ß$_{1a}$ subunit depends upon donor-acceptor position and RyR1 expression. (A) FRET efficiencies for ß$_{1a}$ subunit constructs in myotubes when CFP donor was located at the N-terminus and CCPGCC acceptor site was tested at five different positions of ß$_{1a}$ labeled M1 (construct 8), Q57 (construct 14), P249 (construct 15), H458 (construct 16) and M524 (construct 17), as indicated in schematic above bar graphs. (B) FRET efficiencies for same ß$_{1a}$ subunit constructs in myotubes except the CFP donor was located at the C-terminus (construct 12, 18, 19, 20 and 21). For both panels A and B the ß$_{1a}$ constructs were expressed in wild type (black) or RyR1 KO (gray) myotubes. Only the construct H458-CCGPCC ß$_{1a}$-CFP (construct 21) displayed significant difference FRET efficiency (*p<0.001) in the presence (in WT 0.12 ± 0.01) versus absence (in KO 0.19 ± 0.01) of RyR1 (in Table 1 boxed). (C) Ca^{2+} current expression at test potentials of –30 mV and +30 mV in ß$_1$ KO myotubes expressing H458-CCGPCC ß$_{1a}$-CFP (construct 21) compared to non-transfected (NT) ß KO control which demonstrates that this construct forms functional ß subunits. (D) Comparison of FRET efficiency of H458 CCPGCC ß$_{1a}$-CFP (construct 21) transfected in either WT or dyspedic myotubes. Transfection of RyR1 into dyspedic myotubes eliminated the increase in FRET observed in the absence of RyR1. The RyR1 expression marker (CD8) or the presence of endogenous ß$_{1a}$ subunits has no effect on the measured FRET efficiencies. The FRET efficiency of construct 21 was 0.12 ± 0.01, when it was transfected in either wild type (WT) or ß KO or RyR1 KO cells in presence of RyR1 + CD8 plasmids (triple transfected). Additionally a comparable FRET efficiency observed in RyR1 KO cells between construct 21 alone (0.19 ± 0.01) and construct 21 with CD8 plasmid co-transfection (0.18 ± 0.01), which was significantly higher than the WT (*p<0.001; see results in Table 1) (E) Expression and intramolecular FRET of H458CCPGCC ß$_{1a}$- CFP alone and co-transfected with RyR1 in dyspedic myotubes with the number represents the fluorescence intensity of the region in the myotube and the arrow indicated CD8 beads.

doi:10.1371/journal.pone.0131399.g004

Table 1. FRET efficiency of N-terminal or C-terminal CFP and CCPGCC tagged in different domain of $ß_{1a}$ constructs expressed in WT, dyspedic and $ß_1$ KO myotubes.

cDNA Construct	Transfected Cell Type	No. of cells analyzed	FRET efficiency
CFP-$ß_{1a}$			
Q57 CCPGCC	WT	40	0.30±0.01
(Construct # 14)	RyR1 KO	41	0.32±0.01
P249 CCPGCC	WT	19	0.21±0.03
(Construct # 15)	RyR1 KO	19	0.17±0.01
H458 CCPGCC	WT	35	0.20±0.01
(Construct # 16)	RyR1 KO	23	0.16±0.01
M524 CCPGCC	WT	46	0.15±0.01
$ß_{1a}$-CFP			
M1 CCPGCC	WT	44	0.06±0.01
(Construct # 18)	RyR1 KO	43	0.01±0.01
Q57 CCPGCC	WT	26	0.16±0.01
(Construct # 19)	RyR1 KO	20	0.16±0.02
P249 CCPGCC	WT	33	0.12±0.01
(Construct # 20)	RyR1 KO	30	0.09±0.01
H458 CCPGCC	WT	37	0.12±0.01
(Construct # 21)	RyR1 KO	23	0.19±0.01
H458 CCPGCC	RyR1 KO	34	0.12±0.01
(Construct # 21) + RyR1 + CD8			
H458 CCPGCC	RyR1 KO	31	0.18±0.01
(Construct # 21) + CD8			
H458 CCPGCC	$ß_1$ KO	35	0.12±0.01
(Construct # 21)			

doi:10.1371/journal.pone.0131399.t001

First, we demonstrate that this construct can form functional ß subunits based on its ability to rescue L-type Ca^{2+} currents in $ß_1$ KO myotubes (Fig 4C). To determine if the observed difference between wild type and dyspedic myotubes for the construct H458 CCPGCC- $ß_{1a}$-CFP (construct 21) was specifically due to the absence of RyR1, dyspedic myotubes were transfected with H458 CCPGCC- $ß_{1a}$-CFP (construct 21), wild type RyR1 and CD8 (CD8 to allow detection of the transfected myotubes). The RyR1 + CD8 dyspedic myotubes showed FRET (0.12 ± 0.01) comparable to wild type myotubes (Fig 4D and 4E right panel and Table 1), and expression of CD8 alone in dyspedic myotubes resulted in FRET (0.18 ± 0.01) indistinguishable from nontransfected dyspedic myotubes (Fig 4D). These results support the idea that the RyR1 is the critical difference inducing a conformational change in the $ß_{1a}$ subunit C-terminus. An additional control experiment measured the FRET efficiency of the construct H458 CCPGCC $ß_{1a}$-CFP (construct 1) in $ß_1$ KO myotubes to exclude an effect of native $ß_1$ subunits, and the measured FRET efficiency was similar (0.12 ± 0.01) to that observed in wild type myotubes (0.12 ± 0.01). Overall, these experiments indicate that the C-terminus of the $ß_{1a}$ subunit exhibits significantly different conformations in the presence and the absence of RyR1 in resting myotubes.

Discussion

In the present study, we have demonstrated a conformational change of $ß_{1a}$ induced by RyR1 in native skeletal myotubes using a FlAsH-based *ex vivo* FRET method. The FlAsH-based *ex vivo* FRET assay can report proximity relationships for donor/acceptor pairs in skeletal

myotubes under appropriate experimental (native) conditions. This method also eliminates potential limitations for the use of FlAsH as a FRET acceptor (non-specific binding and limited access to tetracysteine binding sites) for intramolecular FRET. In this study, a robust intramolecular FRET of the DHPR $ß_{1a}$ subunit using 10 different donor/acceptor pairs spanning all domains of the protein demonstrated the relatively compact nature of the protein. Furthermore, the conformation of the DHPR $ß_{1a}$ subunit was specifically altered in the C-terminus by the presence of the RyR1 receptor suggesting an interaction between these two proteins.

Implications for in situ structure of DHPR $ß_{1a}$ subunit

X-ray crystallographic studies defined the structure of the central core of $ß_2$, $ß_3$ and $ß_4$ subunits revealing interlinked SH3 and GK domains representative of members of the MAGUK superfamily of adapter proteins [29–31]. A less ordered domain in between the SH3 and GK domains composed of the variable central domain of ß subunits is comparable to the 'hook' domain described for the related MAGUK protein PSD95, which may be important for interacting with other proteins [51]. The organization of the SH3 and GK domains in the ß subunits takes a more elongated conformation compared to the more compact relationship of these domains in PSD95[31]. Neither the N- nor C-terminal sequences were resolved in these structures and are likely disordered. Despite the fact that the $ß_1$ subunit structure has not been solved, extensive sequence homology between all ß subunit core regions (> 60% identity between $ß_1$ and the other subunits) suggests a comparable structural organization. This identity was exploited to model the structure of the $ß_{1a}$ subunit (Fig 5). The model maintains the core

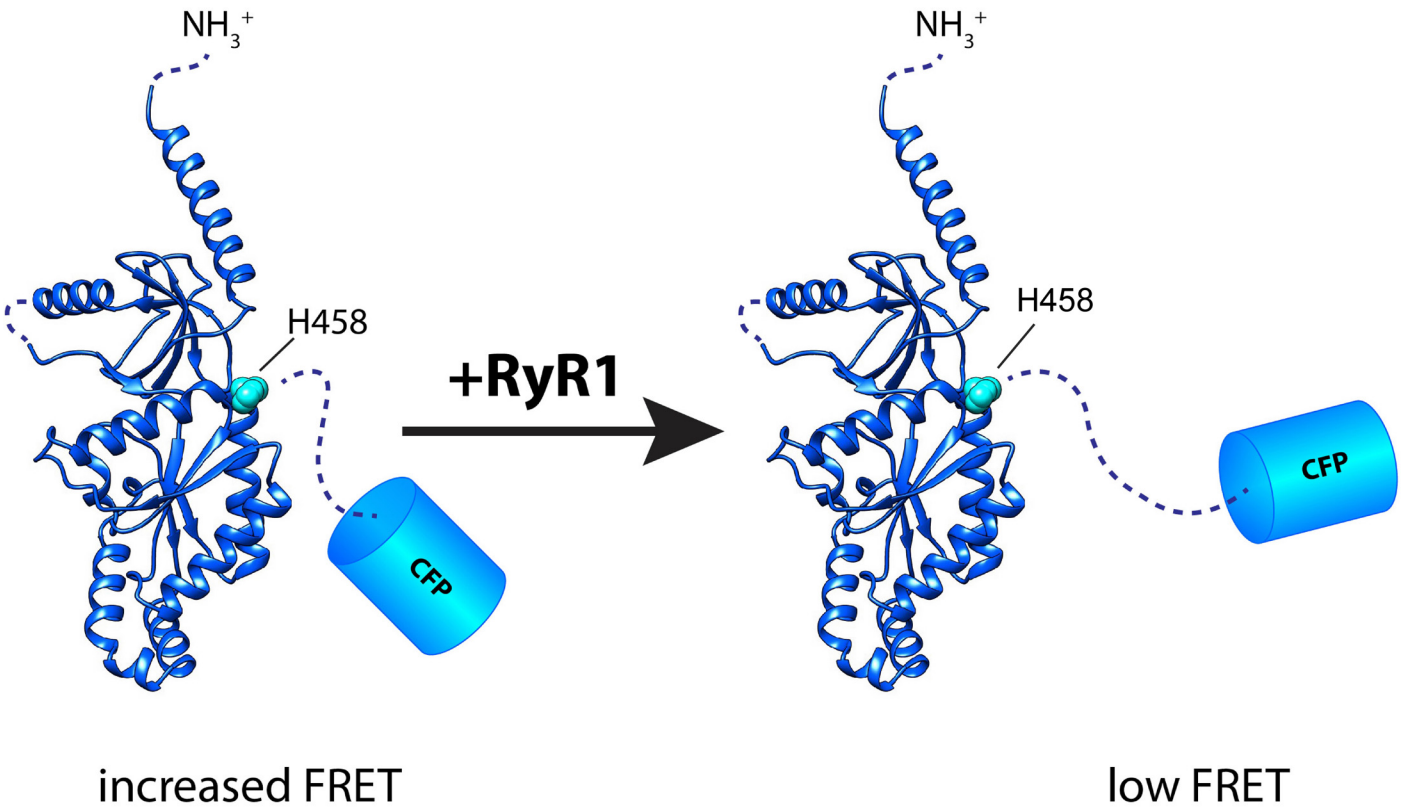

Fig 5. Model of H458 CCPGCC $ß_{1a}$- CFP in a FRET competent state. The $ß_{1a}$ subunit structure was predicted with Phyre2 and obtained using $ß_3$ subunit as a template. The lower FRET between excitation pairs at H458 (CCGPCC) and the C-terminus (CFP) in the presence of RyR1 suggests a structural change wherein the C-terminal region of the modeled $ß_{1a}$ assumes an extended conformation.

doi:10.1371/journal.pone.0131399.g005

domains and properly positions conserved residues at the binding site for the œ interaction domain (AID). Notably, this model also suggests that H458, a CCPGCC insertion site, is the last residue preceding the flexible C-terminus. Thus, the present intramolecular *ex vivo* FRET data for the ß$_{1a}$ subunit can reasonably be compared to the solved crystallographic structures for the ß subunits.

In general, FRET measurements and X-ray crystallography data can provide complementary information on the structural arrangement of a protein. Although the spatial resolution and overall structural detail is less for FRET measurements compared to X-ray diffraction, the unique advantages of FRET include the ability to make measurements in living cells and to detect changes in conformation in response to acute interventions. Because FRET is dependent on both the distance separating the donor and acceptor as well as their relative orientation, it is not possible to calculate absolute changes in distances between donor and acceptor without verifying the orientations [52]. Nevertheless, given the steep dependence (sixth power) of FRET on the distance separating donor and acceptor, it is possible to provide upper limit estimates of distance separating regions in that FRET will not be observed at separations of more than ~10 nm [53]. Because CFP on both the amino and carboxyl termini was able to exhibit FRET from FlAsH-mediated binding to tetracysteine motifs spanning all domains of the ß$_{1a}$ subunit, we conclude that the overall structure of the ß$_{1a}$ subunit is relatively compact with a diameter of less than 10 nm from either the carboxyl or amino terminus. While this is consistent with published structures and our model, this overall architecture cannot be presumed from the crystal structures alone as the native N- and C-termini are absent. Thus, the major new structural information is that *in situ* neither the amino or carboxyl termini are in an extended conformation, but instead they fold over or near the central core region of the ß$_{1a}$ subunit.

DHPR ß subunits have previously been shown to exhibit trans-complementation of the SH3 and GK domains suggesting the formation of dimeric or higher order multimeric complexes of ß subunits [48–50]. In addition, other MAGUK proteins can exhibit intermolecular binding of SH3 and GK domains [54–56], and this type of three-dimensional domain swapping has been described for a variety of proteins [57]. In the case of MAGUKs, multimerization has been proposed to be regulated by factors acting on the HOOK domain between the SH3 and GK domains [54, 55]. However, typically the intramolecular assembly of SH3-GK domains in MAGUKs predominates and effectively competes with the intermolecular SH3-GK interactions [56, 58–60]. For the ß subunits, the biology is intriguing in that not only are full-length ß subunits described, but also truncated ß subunits, which lack the GK domain and carboxyl terminus due to alternative splicing, have been described in native tissues [61–63]. Thus there are multiple possibilities for intermolecular interactions between ß subunits expressed in native cells where a variety of different ß subunit isoforms may be present. However, the current experiments in myotubes did not detect any evidence for intermolecular interactions between full-length ß$_{1a}$ subunits with amino terminus tags. This finding is consistent with the observed stoichiometry of 1:1 for purified DHPR œ$_{1S}$ and ß subunits from skeletal muscle [64]. Nevertheless, regulated intermolecular assembly of different DHPR ß subunit isoforms will likely be an important focus of future study.

Role of ß$_{1a}$ in skeletal excitation-contraction coupling

The core of DHPR ß subunits which includes only the SH3 linked to GK domain has been found to be adequate to recapitulate fundamental functional effects including membrane trafficking of the channel complex as well as modulating voltage-dependent gating [48–50]; however, the full-length ß$_{1a}$ subunit including the carboxyl terminus is required for skeletal type

EC coupling in mouse myotubes [28]. Studies in the zebrafish relaxed mutant, which lacks ß$_{1a}$ protein expression, revealed an essential role of ß$_{1a}$ in the formation of tetrads (groups of four DHPRs) and thus physical DHPR-RyR1 interactions [65]. A unique heptad repeat in the C-terminus of ß$_{1a}$ has been identified as essential for skeletal EC coupling in functional studies [28]. Therefore, a physical contact between C-terminus of the DHPR ß$_{1a}$ and RyR1 has been hypothesized, and consistent with this hypothesis, the C-terminal 35 residues of ß$_{1a}$ with an essential hydrophobic triplet (L^{496}, L^{500} and W^{503}) increase RyR1 channel activity in lipid bilayers [14, 66]. Biochemical pull-down techniques also identified a region of positively charged amino acids in the RyR1 (3495–3502) that specifically interact with the DHPR ß$_{1a}$ [13]. The present study supports a critical functional interaction, in native conditions, between the C-terminus of ß$_{1a}$ and RyR1. FRET between the H458 CCPGCC insertion and the C-terminal CFP significantly increased in RyR1 knockout myotubes (Fig 4B and 4D). This suggests that RyR1 induces a conformational change within ß$_{1a}$ where its C-terminus assumes a more extended structure (i.e. lower FRET state) (Fig 5). This conformational plasticity may be critical between ß$_{1a}$ and RyR1 activities in cytoplasm, and the high degree of sequence diversity within the disordered C-terminus of the different ß subunits may contribute to the specificity of this interaction. However, a previous study using a tandem CFP-YFP reporter inserted at the amino or carboxyl terminal of ß$_{1a}$ revealed a significant change in FRET in myotubes induced by RyR1 expression for the amino terminal tagged construct and not the carboxyl terminal tagged protein, and this contrasts the present results in which there were no differences in FRET for CFP-tetracysteine concatemers expressed at the amino or carboxyl termini [38]. The larger size of the dual fluorescent protein reporter system relative to the CFP-tetracysteine concatemer used in the present *ex vivo* FRET study may contribute to these different results in which general spatial constraints may be apparent only with the larger protein reporter system [36]. Although it was suggested that the amino terminus is more proximal to the RyR1 than the carboxyl terminus, alternative explanations exist in which the overall three dimensional protein complex organization can be altered by RyR1 expression which results in changes in spatial restraints due to a number of associated proteins, e.g. œ$_{1s}$, rather than just proximity to RyR1. A recent study using FRET techniques has indicated that association of I-II loop of DHPR œ(1S) subunit with RyR1 causes reorientation of multiple cytoplasmic domains of the dihydropyridine receptor [8].

A model of skeletal muscle EC coupling is emerging which involves multiple physical contacts between the DHPR complex and RyR1, and one of the essential physical links occurs via the DHPR ß$_{1a}$ subunit. How such links can transmit the voltage-dependent gating conformational changes occurring in the sarcolemmal DHPR œ$_{1s}$ to the RyR1 in the sarcoplasmic reticulum is an important area of future study. Interestingly, structural studies have suggested that ß subunit binding to the AID in the I-II linker of œ subunits can cause a coil to helix transition, which could result in a continuous œ-helix from IS6 through the AID thus providing a relatively rigid physical link between the voltage sensing α subunit and the ß subunit [30, 31]. The present study provides evidence for an interaction between the ß$_{1a}$ subunit and RyR1 in resting myotubyes, but future studies are needed to refine this working model of skeletal EC coupling which may include dynamic intramolecular ß$_{1a}$ subunit FRET measurements during channel gating and determination of intermolecular FRET between DHPR subunits and RyR1.

Author Contributions

Conceived and designed the experiments: DB TJK RCB. Performed the experiments: DB RCB AM. Analyzed the data: DB AM TJK RCB. Contributed reagents/materials/analysis tools: DB AM TJK RCB. Wrote the paper: DB TJK RCB.

References

1. Marty I, Robert M, Villaz M, De Jongh K, Lai Y, Catterall WA, et al. Biochemical evidence for a complex involving dihydropyridine receptor and ryanodine receptor in triad junctions of skeletal muscle. Proceedings of the National Academy of Sciences of the United States of America. 1994; 91(6):2270–4. PMID: 8134386; PubMed Central PMCID: PMC43352.
2. el Hayek R, Antoniu B, Wang J, Hamilton SL, Ikemoto N. Identification of calcium release-triggering and blocking regions of the II-III loop of the skeletal muscle dihydropyridine receptor. The Journal of biological chemistry. 1995; 270(38):22116–8. PMID: 7673188
3. Leong P, MacLennan DH. Complex interactions between skeletal muscle ryanodine receptor and dihydropyridine receptor proteins. BiochemCell Biol. 1998; 76(5):681–94.
4. Leong P, MacLennan DH. The cytoplasmic loops between domains II and III and domains III and IV in the skeletal muscle dihydropyridine receptor bind to a contiguous site in the skeletal muscle ryanodine receptor. The Journal of biological chemistry. 1998; 273(45):29958–64. PMID: 9792715
5. Leong P, MacLennan DH. A 37-amino acid sequence in the skeletal muscle ryanodine receptor interacts with the cytoplasmic loop between domains II and III in the skeletal muscle dihydropyridine receptor. The Journal of biological chemistry. 1998; 273(14):7791–4. PMID: 9525869
6. Sencer S, Papineni RV, Halling DB, Pate P, Krol J, Zhang JZ, et al. Coupling of RYR1 and L-type calcium channels via calmodulin binding domains. The Journal of biological chemistry. 2001; 276 (41):38237–41. doi: 10.1074/jbc.C100416200 PMID: 11500484.
7. Proenza C, O'Brien J, Nakai J, Mukherjee S, Allen PD, Beam KG. Identification of a region of RyR1 that participates in allosteric coupling with the alpha(1S) (Ca(V)1.1) II-III loop. The Journal of biological chemistry. 2002; 277(8):6530–5. PMID: 11726651
8. Polster A, Ohrtman JD, Beam KG, Papadopoulos S. Fluorescence resonance energy transfer (FRET) indicates that association with the type I ryanodine receptor (RyR1) causes reorientation of multiple cytoplasmic domains of the dihydropyridine receptor (DHPR) alpha(1S) subunit. The Journal of biological chemistry. 2012; 287(49):41560–8. doi: 10.1074/jbc.M112.404194 PMID: 23071115; PubMed Central PMCID: PMC3510851.
9. Marty I, Robert M, Villaz M, De Jongh K, Lai Y, Catterall WA, et al. Biochemical evidence for a complex involving dihydropyridine receptor and ryanodine receptor in triad junctions of skeletal muscle. Proc NatlAcadSciUSA. 1994; 91(6):2270–4.
10. Tanabe T, Takeshima H, Mikami A, Flockerzi V, Takahashi H, Kangawa K, et al. Primary structure of the receptor for calcium channel blockers from skeletal muscle. Nature. 1987; 328(6128):313–8. doi: 10.1038/328313a0 PMID: 3037387.
11. Serysheva II, Ludtke SJ, Baker MR, Chiu W, Hamilton SL. Structure of the voltage-gated L-type Ca2+ channel by electron cryomicroscopy. Proc NatlAcadSciUSA. 2002; 99(16):10370–5.
12. Wolf M, Eberhart A, Glossmann H, Striessnig J, Grigorieff N. Visualization of the domain structure of an L-type Ca2+ channel using electron cryo-microscopy. Journal of molecular biology. 2003; 332(1):171–82. PMID: 12946355.
13. Cheng W, Altafaj X, Ronjat M, Coronado R. Interaction between the dihydropyridine receptor Ca2+ channel beta-subunit and ryanodine receptor type 1 strengthens excitation-contraction coupling. Proceedings of the National Academy of Sciences of the United States of America. 2005; 102(52):19225–30. doi: 10.1073/pnas.0504334102 PMID: 16357209; PubMed Central PMCID: PMC1323149.
14. Rebbeck RT, Karunasekara Y, Gallant EM, Board PG, Beard NA, Casarotto MG, et al. The beta(1a) subunit of the skeletal DHPR binds to skeletal RyR1 and activates the channel via its 35-residue C-terminal tail. Biophysical journal. 2011; 100(4):922–30. doi: 10.1016/j.bpj.2011.01.022 PMID: 21320436; PubMed Central PMCID: PMC3037709.
15. Neely A, Wei X, Olcese R, Birnbaumer L, Stefani E. Potentiation by the beta subunit of the ratio of the ionic current to the charge movement in the cardiac calcium channel. Science. 1993; 262(5133):575–8. PMID: 8211185.
16. Castellano A, Wei X, Birnbaumer L, Perez-Reyes E. Cloning and expression of a neuronal calcium channel beta subunit. The Journal of biological chemistry. 1993; 268(17):12359–66. PMID: 7685340.
17. Qin N, Olcese R, Zhou J, Cabello OA, Birnbaumer L, Stefani E. Identification of a second region of the beta-subunit involved in regulation of calcium channel inactivation. The American journal of physiology. 1996; 271(5 Pt 1):C1539–45. PMID: 8944637.
18. Noceti F, Baldelli P, Wei X, Qin N, Toro L, Birnbaumer L, et al. Effective gating charges per channel in voltage-dependent K+ and Ca2+ channels. The Journal of general physiology. 1996; 108(3):143–55. PMID: 8882860; PubMed Central PMCID: PMC2229320.
19. Kamp TJ, Perez-Garcia MT, Marban E. Enhancement of ionic current and charge movement by coexpression of calcium channel beta 1A subunit with alpha 1C subunit in a human embryonic kidney cell

line. The Journal of physiology. 1996; 492 (Pt 1):89–96. PMID: 8730585; PubMed Central PMCID: PMC1158863.

20. Olcese R, Neely A, Qin N, Wei X, Birnbaumer L, Stefani E. Coupling between charge movement and pore opening in vertebrate neuronal alpha 1E calcium channels. The Journal of physiology. 1996; 497 (Pt 3):675–86. PMID: 9003553; PubMed Central PMCID: PMC1160964.
21. Wei SK, Colecraft HM, DeMaria CD, Peterson BZ, Zhang R, Kohout TA, et al. Ca(2+) channel modulation by recombinant auxiliary beta subunits expressed in young adult heart cells. Circulation research. 2000; 86(2):175–84. PMID: 10666413.
22. Colecraft HM, Alseikhan B, Takahashi SX, Chaudhuri D, Mittman S, Yegnasubramanian V, et al. Novel functional properties of Ca(2+) channel beta subunits revealed by their expression in adult rat heart cells. The Journal of physiology. 2002; 541(Pt 2):435–52. PMID: 12042350; PubMed Central PMCID: PMC2290333.
23. Gregg RG, Messing A, Strube C, Beurg M, Moss R, Behan M, et al. Absence of the beta subunit (cchb1) of the skeletal muscle dihydropyridine receptor alters expression of the alpha 1 subunit and eliminates excitation-contraction coupling. Proceedings of the National Academy of Sciences of the United States of America. 1996; 93(24):13961–6. PMID: 8943043; PubMed Central PMCID: PMC19477.
24. Strube C, Beurg M, Powers PA, Gregg RG, Coronado R. Reduced Ca2+ current, charge movement, and absence of Ca2+ transients in skeletal muscle deficient in dihydropyridine receptor beta 1 subunit. Biophysical journal. 1996; 71(5):2531–43. doi: 10.1016/S0006-3495(96)79446-8 PMID: 8913592; PubMed Central PMCID: PMC1233741.
25. Beurg M, Sukhareva M, Ahern CA, Conklin MW, Perez-Reyes E, Powers PA, et al. Differential regulation of skeletal muscle L-type Ca2+ current and excitation-contraction coupling by the dihydropyridine receptor beta subunit. Biophysical journal. 1999; 76(4):1744–56. doi: 10.1016/S0006-3495(99)77336-4 PMID: 10096875; PubMed Central PMCID: PMC1300153.
26. Sheridan DC, Carbonneau L, Ahern CA, Nataraj P, Coronado R. Ca2+-dependent excitation-contraction coupling triggered by the heterologous cardiac/brain DHPR beta2a-subunit in skeletal myotubes. BiophysJ. 2003; 85(6):3739–57.
27. Sheridan DC, Cheng W, Ahern CA, Mortenson L, Alsammarae D, Vallejo P, et al. Truncation of the carboxyl terminus of the dihydropyridine receptor beta1a subunit promotes Ca2+ dependent excitation-contraction coupling in skeletal myotubes. Biophysical journal. 2003; 84(1):220–37. doi: 10.1016/S0006-3495(03)74844-9 PMID: 12524277; PubMed Central PMCID: PMC1302605.
28. Sheridan DC, Cheng W, Carbonneau L, Ahern CA, Coronado R. Involvement of a heptad repeat in the carboxyl terminus of the dihydropyridine receptor beta1a subunit in the mechanism of excitation-contraction coupling in skeletal muscle. BiophysJ. 2004; 87(2):929–42.
29. Chen YH, Li MH, Zhang Y, He LL, Yamada Y, Fitzmaurice A, et al. Structural basis of the alpha1-beta subunit interaction of voltage-gated Ca2+ channels. Nature. 2004; 429(6992):675–80. doi: 10.1038/nature02641 PMID: 15170217.
30. Van Petegem F, Clark KA, Chatelain FC, Minor DL Jr. Structure of a complex between a voltage-gated calcium channel beta-subunit and an alpha-subunit domain. Nature. 2004; 429(6992):671–5. doi: 10.1038/nature02588 PMID: 15141227; PubMed Central PMCID: PMC3076333.
31. Opatowsky Y, Chen CC, Campbell KP, Hirsch JA. Structural analysis of the voltage-dependent calcium channel beta subunit functional core and its complex with the alpha 1 interaction domain. Neuron. 2004; 42(3):387–99. PMID: 15134636.
32. Heidecker M, Yan-Marriott Y, Marriott G. Proximity relationships and structural dynamics of the phalloidin binding site of actin filaments in solution and on single actin filaments on heavy meromyosin. Biochemistry. 1995; 34(35):11017–25. PMID: 7669759
33. Griffin BA, Adams SR, Tsien RY. Specific covalent labeling of recombinant protein molecules inside live cells. Science. 1998; 281(5374):269–72. PMID: 9657724.
34. Griffin BA, Adams SR, Jones J, Tsien RY. Fluorescent labeling of recombinant proteins in living cells with FlAsH. Methods in enzymology. 2000; 327:565–78. PMID: 11045009.
35. Hoffmann C, Gaietta G, Bunemann M, Adams SR, Oberdorff-Maass S, Behr B, et al. A FlAsH-based FRET approach to determine G protein-coupled receptor activation in living cells. Nature methods. 2005; 2(3):171–6. doi: 10.1038/nmeth742 PMID: 15782185.
36. Bhattacharya D, Ansari IH, Mehle A, Striker R. Fluorescence resonance energy transfer-based intracellular assay for the conformation of hepatitis C virus drug target NS5A. Journal of virology. 2012; 86 (15):8277–86. doi: 10.1128/JVI.00645-12 PMID: 22623794; PubMed Central PMCID: PMC3421644.
37. Bhattacharya D, Ansari IH, Hamatake R, Walker J, Kazmierski WM, Striker R. Pharmacological disruption of hepatitis C NS5A protein intra- and intermolecular conformations. The Journal of general virology. 2014; 95(Pt 2):363–72. doi: 10.1099/vir.0.054569–0 PMID: 23997183.

38. Papadopoulos S, Leuranguer V, Bannister RA, Beam KG. Mapping sites of potential proximity between the dihydropyridine receptor and RyR1 in muscle using a cyan fluorescent protein-yellow fluorescent protein tandem as a fluorescence resonance energy transfer probe. The Journal of biological chemistry. 2004; 279(42):44046–56. PMID: 15280389

39. Miyawaki A, Tsien RY. Monitoring protein conformations and interactions by fluorescence resonance energy transfer between mutants of green fluorescent protein. Methods Enzymol. 2000; 327:472–500. PMID: 11045004

40. Stroffekova K, Proenza C, Beam KG. The protein-labeling reagent FLASH-EDT2 binds not only to CCXXCC motifs but also non-specifically to endogenous cysteine-rich proteins. Pflugers Archiv: European journal of physiology. 2001; 442(6):859–66. PMID: 11680618

41. Takeshima H, Iino M, Takekura H, Nishi M, Kuno J, Minowa O, et al. Excitation-contraction uncoupling and muscular degeneration in mice lacking functional skeletal muscle ryanodine-receptor gene. Nature. 1994; 369(6481):556–9. doi: 10.1038/369556a0 PMID: 7515481.

42. Adams SR, Campbell RE, Gross LA, Martin BR, Walkup GK, Yao Y, et al. New biarsenical ligands and tetracysteine motifs for protein labeling in vitro and in vivo: synthesis and biological applications. Journal of the American Chemical Society. 2002; 124(21):6063–76. PMID: 12022841.

43. Beurg M, Sukhareva M, Strube C, Powers PA, Gregg RG, Coronado R. Recovery of Ca2+ current, charge movements, and Ca2+ transients in myotubes deficient in dihydropyridine receptor beta 1 subunit transfected with beta 1 cDNA. Biophysical journal. 1997; 73(2):807–18. doi: 10.1016/S0006-3495(97)78113-X PMID: 9251797; PubMed Central PMCID: PMC1180977.

44. Ahern CA, Sheridan DC, Cheng W, Mortenson L, Nataraj P, Allen P, et al. Ca2+ current and charge movements in skeletal myotubes promoted by the beta-subunit of the dihydropyridine receptor in the absence of ryanodine receptor type 1. Biophysical journal. 2003; 84(2 Pt 1):942–59. PMID: 12547776; PubMed Central PMCID: PMC1302672.

45. Schneider CA, Rasband WS, Eliceiri KW. NIH Image to ImageJ: 25 years of image analysis. Nature methods. 2012; 9(7):671–5. PMID: 22930834.

46. Yan Y, Marriott G. Analysis of protein interactions using fluorescence technologies. Current opinion in chemical biology. 2003; 7(5):635–40. PMID: 14580569.

47. Kelley LA, Sternberg MJ. Protein structure prediction on the Web: a case study using the Phyre server. Nature protocols. 2009; 4(3):363–71. doi: 10.1038/nprot.2009.2 PMID: 19247286.

48. Opatowsky Y, Chomsky-Hecht O, Kang MG, Campbell KP, Hirsch JA. The voltage-dependent calcium channel beta subunit contains two stable interacting domains. The Journal of biological chemistry. 2003; 278(52):52323–32. doi: 10.1074/jbc.M303564200 PMID: 14559910.

49. Takahashi SX, Miriyala J, Colecraft HM. Membrane-associated guanylate kinase-like properties of beta-subunits required for modulation of voltage-dependent Ca2+ channels. Proceedings of the National Academy of Sciences of the United States of America. 2004; 101(18):7193–8. doi: 10.1073/pnas.0306665101 PMID: 15100405; PubMed Central PMCID: PMC406488.

50. McGee AW, Nunziato DA, Maltez JM, Prehoda KE, Pitt GS, Bredt DS. Calcium channel function regulated by the SH3-GK module in beta subunits. Neuron. 2004; 42(1):89–99. PMID: 15066267.

51. Tavares GA, Panepucci EH, Brunger AT. Structural characterization of the intramolecular interaction between the SH3 and guanylate kinase domains of PSD-95. MolCell. 2001; 8(6):1313–25.

52. Nagai T, Yamada S, Tominaga T, Ichikawa M, Miyawaki A. Expanded dynamic range of fluorescent indicators for Ca(2+) by circularly permuted yellow fluorescent proteins. Proceedings of the National Academy of Sciences of the United States of America. 2004; 101(29):10554–9. doi: 10.1073/pnas.0400417101 PMID: 15247428; PubMed Central PMCID: PMC490022.

53. dos Remedios CG, Moens PD. Fluorescence resonance energy transfer spectroscopy is a reliable "ruler" for measuring structural changes in proteins. Dispelling the problem of the unknown orientation factor. Journal of structural biology. 1995; 115(2):175–85. doi: 10.1006/jsbi.1995.1042 PMID: 7577238.

54. Hough CD, Woods DF, Park S, Bryant PJ. Organizing a functional junctional complex requires specific domains of the Drosophila MAGUK Discs large. Genes & development. 1997; 11(23):3242–53. PMID: 9389655; PubMed Central PMCID: PMC316757.

55. McGee AW, Dakoji SR, Olsen O, Bredt DS, Lim WA, Prehoda KE. Structure of the SH3-guanylate kinase module from PSD-95 suggests a mechanism for regulated assembly of MAGUK scaffolding proteins. Molecular cell. 2001; 8(6):1291–301. PMID: 11779504.

56. Nix SL, Chishti AH, Anderson JM, Walther Z. hCASK and hDlg associate in epithelia, and their src homology 3 and guanylate kinase domains participate in both intramolecular and intermolecular interactions. The Journal of biological chemistry. 2000; 275(52):41192–200. doi: 10.1074/jbc.M002078200 PMID: 10993877.

57. Liu Y, Eisenberg D. 3D domain swapping: as domains continue to swap. Protein science: a publication of the Protein Society. 2002; 11(6):1285–99. doi: 10.1110/ps.0201402 PMID: 12021428; PubMed Central PMCID: PMC2373619.

58. McGee AW, Bredt DS. Identification of an intramolecular interaction between the SH3 and guanylate kinase domains of PSD-95. The Journal of biological chemistry. 1999; 274(25):17431–6. PMID: 10364172.

59. Wu H, Reissner C, Kuhlendahl S, Coblentz B, Reuver S, Kindler S, et al. Intramolecular interactions regulate SAP97 binding to GKAP. EMBO J. 2000; 19(21):5740–51. PMID: 11060025

60. Shin H, Hsueh YP, Yang FC, Kim E, Sheng M. An intramolecular interaction between Src homology 3 domain and guanylate kinase-like domain required for channel clustering by postsynaptic density-95/SAP90. JNeurosci. 2000; 20(10):3580–7.

61. Cohen RM, Foell JD, Balijepalli RC, Shah V, Hell JW, Kamp TJ. Unique modulation of L-type Ca2+ channels by short auxiliary beta1d subunit present in cardiac muscle. Am J Physiol Heart CircPhysiol. 2005; 288(5):H2363–H74.

62. Foell JD, Balijepalli RC, Delisle BP, Yunker AM, Robia SL, Walker JW, et al. Molecular heterogeneity of calcium channel beta-subunits in canine and human heart: evidence for differential subcellular localization. Physiological genomics. 2004; 17(2):183–200. PMID: 14762176

63. Hibino H, Pironkova R, Onwumere O, Rousset M, Charnet P, Hudspeth AJ, et al. Direct interaction with a nuclear protein and regulation of gene silencing by a variant of the Ca2+-channel beta 4 subunit. ProcNatlAcadSciUSA. 2003; 100(1):307–12.

64. Leung AT, Imagawa T, Block B, Franzini-Armstrong C, Campbell KP. Biochemical and ultrastructural characterization of the 1,4-dihydropyridine receptor from rabbit skeletal muscle. Evidence for a 52,000 Da subunit. JBiolChem. 1988; 263(2):994–1001.

65. Schredelseker J, Di B, V, Obermair GJ, Felder ET, Flucher BE, Franzini-Armstrong C, et al. The beta 1a subunit is essential for the assembly of dihydropyridine-receptor arrays in skeletal muscle. ProcNatlAcadSciUSA. 2005; 102(47):17219–24.

66. Karunasekara Y, Rebbeck RT, Weaver LM, Board PG, Dulhunty AF, Casarotto MG. An alpha-helical C-terminal tail segment of the skeletal L-type Ca2+ channel beta1a subunit activates ryanodine receptor type 1 via a hydrophobic surface. FASEB journal: official publication of the Federation of American Societies for Experimental Biology. 2012; 26(12):5049–59. doi: 10.1096/fj.12-211334 PMID: 22962299.